ORIGINAL CONTRIBUTION

Hysteresis controlled water droplet splitting on superhydrophobic paper

Lester Li · Victor Breedveld ·
Dennis W. Hess

Abstract Fabrication of surfaces with heterogeneous contact angle hysteresis enables extraction of droplet samples from bulk liquid volumes. These surfaces are created by printing high hysteresis wax islands onto low hysteresis superhydrophobic paper. The volume of the sampled droplets depends on the hysteresis of the printed islands, which can be controlled through both physical and chemical means. Physically, hysteresis is modified through the addition of surface roughness. Chemical hysteresis is tuned by changing the active chemical groups present on the wax surface. The observed control of the volume of sampled droplets, which is necessary for quantitative biochemical or chemical assays, extends to scenarios in which multiple droplet samples are extracted simultaneously from a single bulk droplet. Demonstration of the capacity of this technique to perform colorimetric glucose immunoassays is described. The ability to obtain well-defined microliter sample volumes and to extract several samples simultaneously from the same source enables the development of two-dimensional paper-based microfluidic devices for biomedical testing.

L. Li · V. Breedveld · D. W. Hess (✉)
School of Chemical and Biomolecular Engineering,
Georgia Institute of Technology,
311 Ferst Drive,
Atlanta, GA 30332, USA
e-mail: dennis.hess@chbe.gatech.edu

L. Li
Institute of Paper Science and Technology,
Georgia Institute of Technology,
500 10th Street Northwest,
Atlanta, GA 30318, USA

Introduction

The potential applications of superhydrophobic (SH) surfaces in numerous fields has drawn much attention from the scientific community [1–7]. An SH surface is defined as one with an apparent water contact angle (CA) larger than 150° so that water droplets bead up to minimize contact with the surface. Within the field of superhydrophobicity, there exist two types of observed behaviors with regards to droplet mobility, "roll-off" and "sticky" SH surfaces, which differ greatly in the degree of droplet adhesion. These two regimes are generally characterized through contact angle hysteresis, which is defined as the difference between the advancing and receding CAs. The fabrication and study of these surfaces often mimic and attempt to improve upon SH surfaces that exist in nature. For example, the lotus leaf exhibits roll-off SH properties, defined as having an advancing CA>150°, with a CA hysteresis <10° [8–11]. Rose petals, on the other hand, also have an advancing CA>150°, but with a CA hysteresis >10°, making them a sticky SH surface [12, 13]. The ability to fabricate SH substrates with tunable hysteresis has been demonstrated on surfaces such as silicon [13–15], metals [16, 17] and polymers [18, 19]. Previous work from our group has demonstrated the ability to tune the hysteresis on cellulosic structures from sticky to roll-off while maintaining an advancing CA>150° [20, 21].

CA hysteresis occurs when the energy needed to separate a liquid and a solid interface exceeds the energy required to form a new interface [22]. Thus, manipulation of the hysteresis of a substrate is dependent on the ability to tune the interfacial interactions between the solid and the liquid phases through either chemical or physical surface modifications. Chemically, hysteresis is defined as an interaction

that causes molecules at the interface to arrange differently when in contact with the liquid [22, 23]. This form of hysteresis typically occurs on surfaces that have both polar and non-polar groups, such as surfactants. Physical or mechanical hysteresis occurs by increasing the contact area between a surface and liquid. The most common approach is the addition of roughness to a surface, which increases the overall surface area. If the liquid wets the additional surface area, the increased interaction results in higher hysteresis. However, the combination of surface roughness at both micro and nano-length scales can decrease wetting as well, in which case hysteresis is reduced.

By combining areas of high and low hysteresis on a single heterogeneous substrate, preferential adhesion of droplets to specific areas on the substrate can be achieved, and droplet mobility can be manipulated [24]. Wang et al. fabricated heterogeneous SH surfaces using carbon nanotubes. Subsequently, they showed that they could preferentially adhere droplets to specific areas of the SH surface by drawing patterns on it with a pencil, thus effectively covering the nanotubes with graphite [25]. Leopoldes et al. demonstrated preferential adherence of liquid jetted onto a chemically heterogeneous matrix of hydrophobic and hydrophilic areas [26]; based on their report, it appears that they not only varied contact angle, but also varied hysteresis by terminating the surface with either hydrophilic carboxyl groups (high hysteresis) or hydrophobic methyl groups (low hysteresis). Our research group has demonstrated control of droplet mobility on a surface by printing high hysteresis wax islands onto low hysteresis SH paper [27, 28]. The preferential adhesion of droplets to the high hysteresis islands makes it possible to store, mix and sample droplets. It was proposed that controlled manipulation of droplets on the surface of SH paper through wax pattern designs could yield two-dimensional microfluidic devices that are particularly attractive due to the versatility and ease of the printing method. Termed Hysteresis Enabled Lab on Paper (HELP), the proposed devices could enable inexpensive point-of-care diagnostics that would allow further off-site testing of liquid samples if needed. In order to perform accurate biomedical testing, it is crucial that sample volumes are well-defined and reproducible so that quantitative reactions with chemical reagents are possible, in particular if concentrations of analytes must be determined with high confidence levels. For example, there has recently been increased interest in the simultaneous testing for multiple illnesses from one droplet of bodily liquid on a single device [29]. In order to facilitate such characterizations, a bulk droplet must be split into several smaller droplets prior to the analytical reactions; lack of droplet volume reproducibility will directly affect the outcomes of the testing.

In this paper, we present an approach to the sampling of small droplets from a larger bulk droplet by controlling CA

hysteresis. Fabrication of a high hysteresis pattern on low hysteresis SH paper enables control of the volume of the sampled droplet depending on the magnitude of the hysteresis. We control hysteresis, and thus volume sampled, through both chemical and physical surface modifications and show that the result of both approaches is fundamentally the same. This level of control will enable extraction of single and multiple sample droplets from a bulk droplet for biomedical testing.

Methodology

Superhydrophobic paper

Paper handsheets were prepared according to the TAPPI standardized method T205 sp-02 using a 50/50 mixture of southern softwood kraft and southern hardwood kraft pulp. Superhydrophobic properties were established by etching the handsheets using oxygen in a parallel plate RF (13.56 MHz) plasma reactor for 45 min, followed by the deposition of ~100 nm of fluorocarbon from a pentafluoroethane precursor (Praxair). Further details regarding the process parameters and reactor configuration during the fabrication of SH paper substrates can be found elsewhere [20].

Printed patterns

Printing of the desired patterns was performed via a thermal transfer printing technique, using paraffin wax (Spectrum Chemical Mfg Corp., New Brunswick, NJ), carnauba wax (Alfa Aesar), stearic acid (Fluka, >97.0 %) and mixtures thereof. Carnauba wax was selected due to its low apparent CA (97.3°±2.3) relative to other waxes to help maximize adhesion; paraffin wax and stearic acid were chosen based on their degree of polarity, lower and higher than carnauba wax, respectively. A transfer sheet was prepared by melting the wax of choice and then dip-coating a slip of standard copy paper into the liquid wax. Machined aluminum stamps with single-dot and multiple-dot patterns were created as shown in Figs. 1 and 2. The dimensions of the patterns were
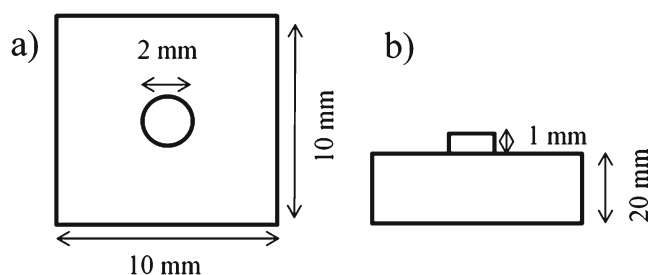
Fig. 1 *Single dot* stamp design dimensions. **a** Vertical view and **b** side view
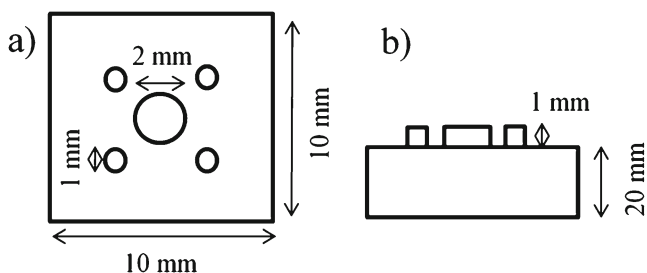
Fig. 2 *Multiple dot* stamp design dimensions. **a** Vertical view and **b** side view

chosen such that compression of a typical bulk droplet (50–100 μL) between the paper sheets results in an expansion of its diameter well beyond the edges of the printed pattern; the longest (diagonal) dimension of the largest pattern, the multiple-dot design, was 5.65 mm. Figure 3 shows the transfer printing procedure using the stamp and transfer sheet. The wax dip-coated sheet and the SH sheet that needed to be printed were stacked on top of a glass slide with the SH side facing down, away from the wax-impregnated sheet. The metal stamp, heated to a temperature above the melting point of the wax, was then pressed onto the stack and held down for 3–4 s, while the wax melted, absorbed into the SH sheet and solidified in the shape of the stamp on the glass side of the printed sheet. The procedure resulted in a uniform wax coating throughout the depth of the sheet, with a coating of ~10 μm covering the surface fibers (based on SEM images).

The insolubility of the waxes in water made it possible to reuse samples for ten water droplet sampling experiments, so that reproducibility statistics and experimental error estimates could be established. However, stearic acid's solubility in water limited use of those substrates to no more than two experiments, with further sampling resulting in small but noticeable droplet volume inconsistencies.

Physical roughness was added to the wax surface on the printed substrates by pressing the cooled wax onto various grades of sandpaper. Sandpaper roughness is characterized via the grit number that is specified through the Coated Abrasive Manufacturers Institute (CAMI) standards, with higher grit numbers corresponding to finer particles. The sheets we used (Norton brand; Saint-Gobain Abrasives, Stephenville, TX) were manufactured using aluminum oxide particles (with grit numbers of 100, 150, 220, 320, 400 and 600) and silicon particles (for the 1200 grit paper).
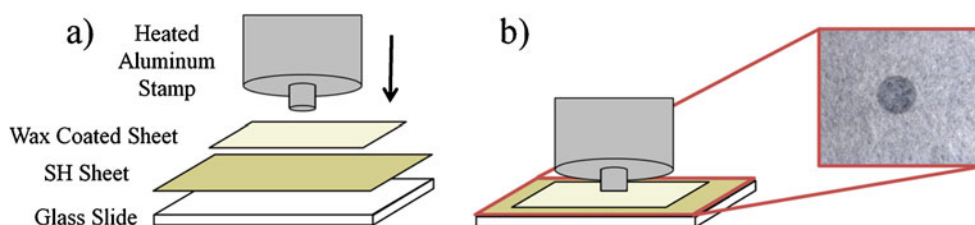
X-ray photoelectron spectroscopy was performed on the patterned SH paper samples before and after pressing with sandpaper to ensure that no transfer of grit particles to the wax had occurred; in these tests, no presence of Si or Al could be detected on the roughened wax surfaces.
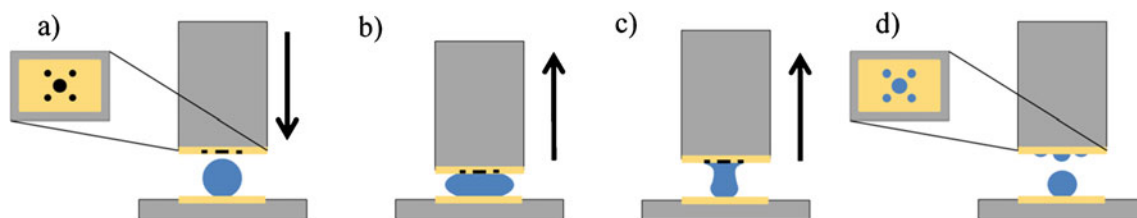
Droplet sampling

Sampling tests were conducted using a squeeze testing unit that moves a platform vertically to compress a 100 μl bulk droplet between two SH sheets, as illustrated in Fig. 4. An important component with regards to the consistency of droplet transfer is the parallelism of the two sheets, which is needed to avoid uneven droplet compression and release. In order to achieve the necessary parallelism, the vertical slide is attached to a base plate with three adjustable screws that enable adjustment of the top plate in relation to the bottom platform on which the bulk droplet rests. The rebound of the vertical slide occurs in ~0.5 s and is controlled by a spring that is compressed as the slide is moved downward. Droplet splitting is observed to occur in three steps: (1) compression of the droplet, (2) necking of the droplet, and (3) pinch-off. These steps can be seen in Fig. 4b, c, d, respectively.

Image analysis

After the transfer is complete, the top plate, along with the vertical slide and patterned sheet are inverted and an image taken of the sample droplets using a Lumenera LU135c camera, equipped with a Leica A6 APO zoom lens. Images are taken at an angle of ~15° relative to the horizontal plane, so that it is possible to view all the droplets at once on a multi-dot design array, while obtaining accurate data on the droplet dimensions. The resulting image is analyzed using the image analysis software package IDL (ITT Visual Information Solutions, Boulder, CO), which measures the lengths of the major and minor axes of the drop through user inputs. From the lengths of the major and minor axes of the droplet, its volume can be calculated using Eq. (1); V is the volume, h the height of the droplet, and c the radius of the contact line between droplet and paper.

$$V = \frac{\pi}{6} h (3c^2 + h^2) \tag{1}$$

Fig. 3 Stamping procedure. **a** Wax-coated sheet and SH sheet stack on top of a glass slide. **b** Heated stamp pressed into the stack; wax melts through the SH paper in the shape of the stamp

Fig. 4 Squeeze test procedure. **a** Droplet between two SH pieces of paper; the *top paper* has a printed design. **b** Droplet is compressed and released. **c** Droplet forms a neck. **d** Droplet splits and water samples are transferred onto printed pattern

Calibration tests with droplets of known volumes established the accuracy of this image analysis procedure for droplets of various sizes and CAs as ±0.03 μL. Each data point presented in this paper is the average of 40–80 droplet splitting experiments and error bars in the graphs represent the standard deviation.

Contact angle measurement

Apparent (static) contact angles were measured with a Rame-Hart contact angle goniometer (Model 100, Netcong, NJ) using 4 μL water droplets. Advancing contact angles were measured using a 2-μL droplet and increasing the volume by 1 μL increments until the volume reached 10 μL. Receding contact angles were measured using a 5-μL droplet and decreasing the volume by 0.5 μL until the volume reached 2 μL.

Substrates for CA measurements of the various wax materials were prepared by melting the pure and mixed solid waxes and dip-coating slips of standard copy paper. For the measurement of physically modified hysteresis, the wax-coated slips of paper were pressed against sandpaper after cooling.

SEM images

Scanning electron microscope (SEM) micrographs were obtained with a Hitachi S-3700N VP-SEM, using the variable pressure mode at a pressure of 80 Pa and an operating voltage of 15 kV.

Profilometry

Roughness data were obtained using a Wyko Optical Profilometer NT2000. Four measurements were taken for each sample and analyzed using the Vison32 (Vecco Instruments Inc.) analysis software. The average roughness, R_a, is calculated as per the ANSI B46.1 standard and the mean peak spacing, S_m, is defined as the mean spacing between peaks along the measured line profile.

Glucose experiments

The reagents for colorimetric glucose experiments were prepared by pipetting 1 μL of 645 U/mL glucose oxidase (Sigma Aldrich), 1 μL of 339 U/mL horseradish peroxidase (Sigma Aldrich) and 0.5 μL of a 2:1 molar mixture of 3,5 dichloro-2-hydroxy-benzenesulfonate (Sigma Aldrich) and 4-aminoantipyrine (Sigma Aldrich) onto each of the four perimeter islands of the multi-dot design. The reagents were allowed to dry overnight on the islands in a dry box. Sampling experiments were conducted using the procedure outlined above with 100 μL droplets of 0.0015 and 0.005 M glucose solutions prepared by dissolving D-glucose (Sigma Aldrich) in DI water.

Results and discussion

Chemical hysteresis

Figure 5 presents the dynamic CAs and the CA hysteresis for homogeneous substrates of five different waxes: pure paraffin wax, a 1:1 mixture (by mass) of carnauba and paraffin wax, pure carnauba wax, a 1:1 mixture of carnauba wax and stearic acid, and pure stearic acid. While the advancing CA of each of the solids is similar, the hysteresis varies widely. The variation in hysteresis is due to differences in the chemical compositions of the materials. Paraffin wax is largely composed of straight chain saturated alkanes ranging from 20 to 40 carbons in length [30]. Carnauba wax, on the other hand, is composed of alkanes, along with aliphatic esters, monohydric alcohols and acids 25 to 30 carbons in length [31]. The esters, alcohols and acids found in carnauba wax have a stronger interaction with water than do the non-polar alkanes that make up paraffin wax. This enhanced interaction results in a chemically increased CA hysteresis for carnauba wax relative to paraffin wax. The 1:1 mixture of carnauba and paraffin waxes exhibits a higher than expected hysteresis close to that of pure carnauba wax. Due to the amorphous and crystalline structures of carnauba and paraffin waxes, respectively, and the differences in melting points, 82–86 °C for carnauba and 47–65 °C for paraffin, phase separation of the waxes could occur upon solidification. Alternatively, it is expected that the addition of paraffin wax alkanes to carnauba wax will result in a change in packing of surface groups, which may influence the hysteresis. While the exact cause of the increased CA

Fig. 5 Plots of advancing and receding CAs and CA hysteresis of several sample types
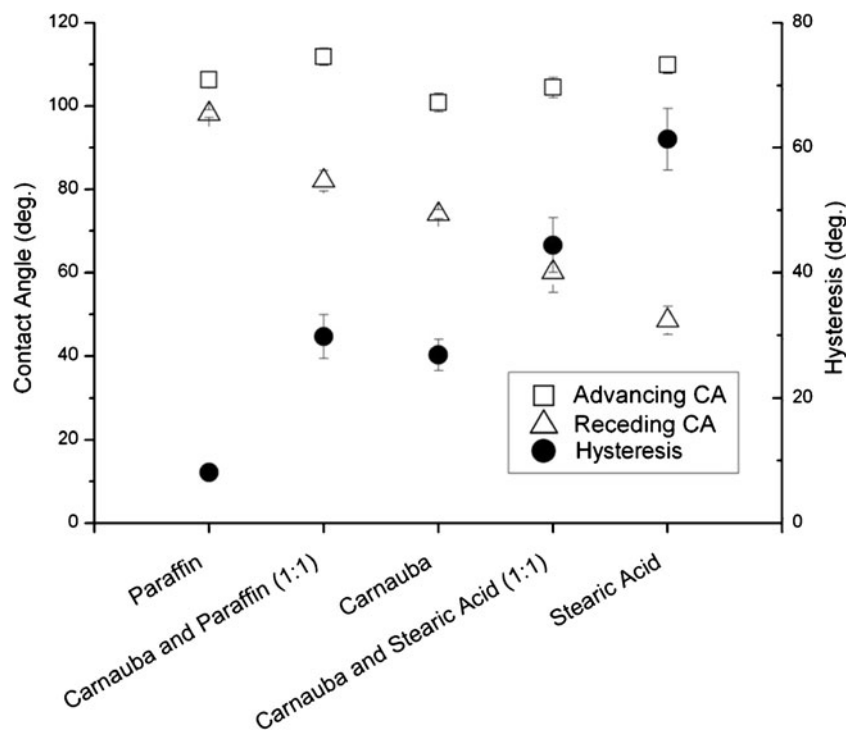
hysteresis is unclear, the low variability observed in hysteresis measurements suggests that if surface heterogeneity exists, it must be at a length scale much smaller than that of the droplet. Stearic acid not only has the shortest chain length of the pure substances, 18 carbons in length, but also is entirely composed of molecules with polar groups. These factors cause stearic acid to have the strongest interaction with water, and thus the highest hysteresis.

Using the wax materials indicated in Fig. 5, single-dot designs were fabricated on low hysteresis SH paper and droplet splitting was used to extract samples from bulk droplets of DI water. The sampled volumes are presented in Fig. 6; clearly, the droplet volume depends upon the chemical hysteresis, with increasing droplet sizes for larger hysteresis values. To illustrate the difference in sampled droplets more clearly, images from the droplet splitting experiments are shown in Fig. 6. As hysteresis is increased, both the lateral and vertical dimensions of the sampled droplet increase.
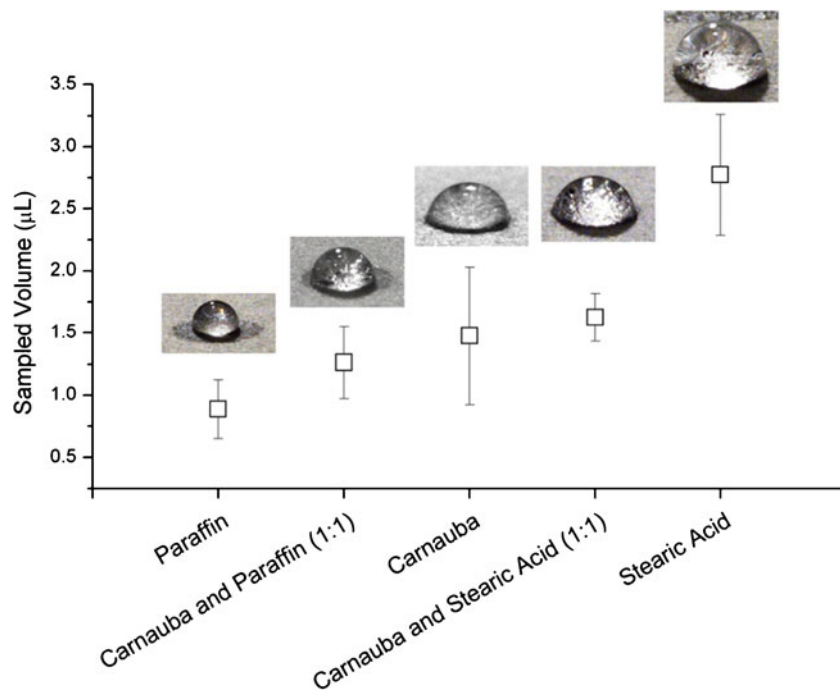
Physical hysteresis

In order to modify the physical hysteresis of printed substrates, surface roughness was added to the printed wax dots. The substrates for studying physical hysteresis were fabricated using pure carnauba wax. By pressing the cooled wax designs against various grades of sandpaper, the wax deformed and generated a range of physical surface roughness. Figure 7 shows SEM images of a selection of carnauba wax designs on SH paper before and after pressing against

various grades of sandpaper. The correlation between grit number and CAMI average particle size on the sandpaper surface can be found in Table 1. For the larger particles, corresponding to lower grit numbers (100–220), the pressing not only deforms the wax, but also significantly deforms the fibers (Fig. 7b, c).

Figure 8 shows that the hysteresis increases as the grit number increases and particle size decreases, while advancing contact angles remain approximately constant. This indicates that the scale of the physical roughness is an important factor in the increase of hysteresis. Johnson and Dettre have performed detailed analysis on the effect of surface roughness on CA hysteresis [32]. Their findings suggested that at certain length scales, increased surface roughness yields an increase in hysteresis. Bhushan et al. studied CA hysteresis on an array of silicon pillars [33]. These authors found that hysteresis was dependent on a nondimensional spacing factor S_f, which was defined as the ratio of the pillar diameter to the distance between the pillar centers. With the sandpaper, not only is the size of the particle changed as the grit number changes, thus changing the amplitude of the roughness, but the mean distance between the particles is varied as well. The average roughness (R_a), along with the mean peak spacing (S_m) for the tested sandpaper grades, is shown in Table 1. Initially, with coarser grits of sandpaper, the distance between the particle peaks, and therefore the indentations, is too large to have an effect on the CA hysteresis. As the particles become smaller, the spacing between indentations decreases. At this lowered length scale, the added physical roughness starts to affect

Fig. 6 Sampled volumes for several types of waxes used for printing; pattern was a 2-mm diameter *circle*


CA hysteresis. Much like the case of increasing chemical hysteresis (Fig. 6), the increase of physical hysteresis also increases the sampled volume, as seen in Fig. 9.

Relationship between sampled volume and hysteresis

Comparison of Figs. 6 and 9 indicates that the sampled droplet volume increases with hysteresis, independent of the method used to modify this surface property. To further test this hypothesis, Fig. 10 presents the volume of sampled droplets obtained through splitting for both chemical and physical surface modification methods against the wax

substrate hysteresis. Good agreement is observed between the two sets of data. A least squared linear regression line is also shown in Fig. 10, further demonstrating the strong correlation between the sampled volume and the hysteresis.

The similarity between the two methods of hysteresis control is a result of the underlying physics that governs the splitting of a bulk droplet. During the droplet release phase (Fig. 4b, c), the bulk droplet effectively recedes across the top sheet. On a zero hysteresis upper surface, the droplet continues receding unhindered, and no splitting is expected to occur due to gravity and surface tension. By adding patterned wax islands with high hysteresis to a low
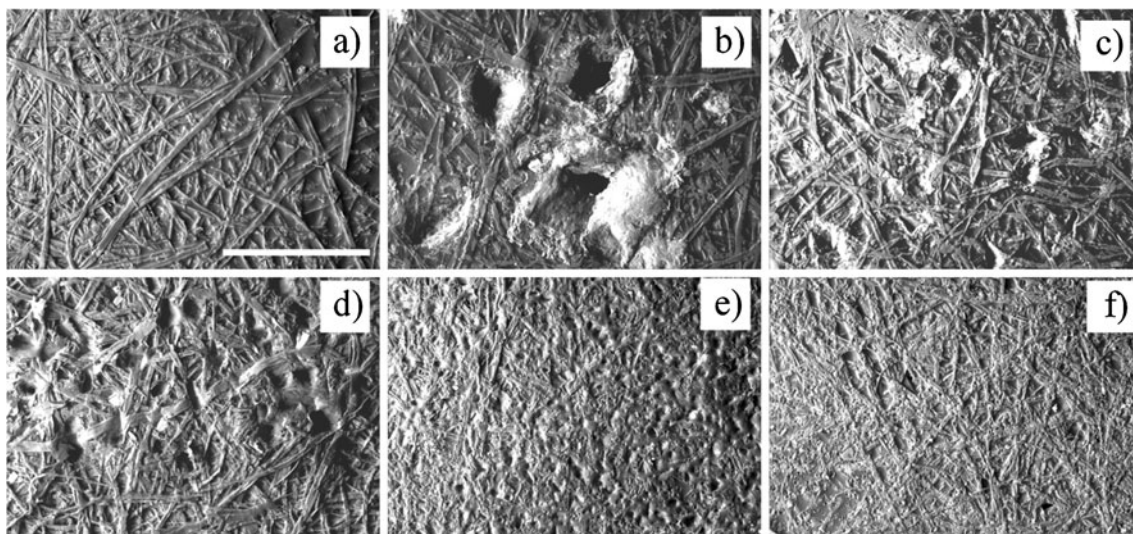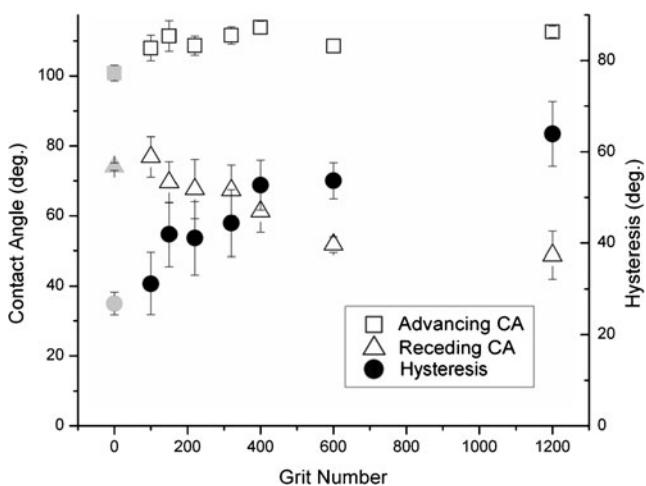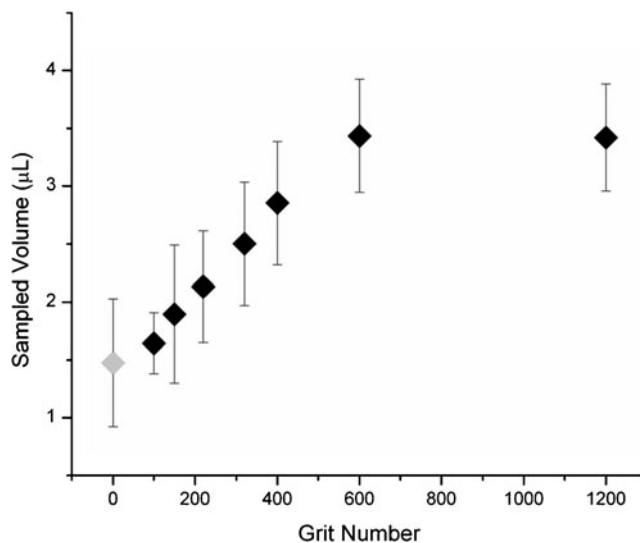

Fig. 7 SEM images of carnauba wax on low hysteresis SH paper after being imprinted with various grades of sand paper: **a** untreated reference, **b** 100 grit, **c** 150 grit, **d** 220 grit, **e** 600 grit, and **f** 1,200 grit. *Scale bar* represents 500 μm
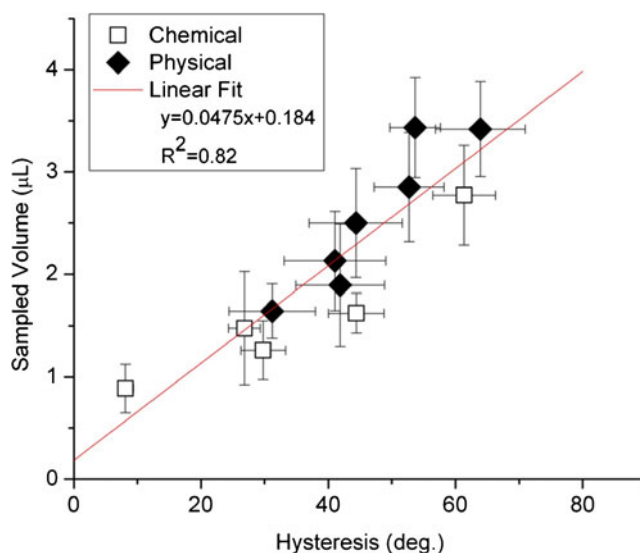
Table 1 Correlation of sandpaper grit designation to average particle size (according to CAMI standard), and the average roughness (R_a) and mean spacing (S_m) measured via profilometry

CAMI Grit Designation	100	150	220	320	400	600	1,200
Average particle size (µm)	140	92	68	36	23	16	6.5
R_a (µm)		24.1	13.8	13.7	10.5	7.5	5.6	3.6
S_m (µm)		57.6	56.8	17.3	16.7	15.1	14	11.3

hysteresis surface, the droplet is able to recede easily across the top surface until it encounters the edges of the printed wax dots. The difference in hysteresis between the surrounding SH paper and the wax pattern results in an additional force that enables droplet splitting. While gravity pulls the droplet downward, away from the top surface, and surface tension resists the deformation of the bulk droplet from its spherical ground state, the adhesion force due to the hysteresis of the wax pattern favors droplet splitting. The end result of this force balance depends on the remaining contact area, i.e., size of the wax pattern and location of droplet breakup. Previous study showed that during transfer of bulk droplets between low hysteresis surfaces and high hysteresis wax islands, the droplets were always pinned at the circumference of the printed dot. Furthermore, the maximum droplet volume that could be transferred was a function of the dot size, as predicted through a simple force balance [27]. In this investigation, however, we study the splitting of bulk droplets and show that the contact angle hysteresis of the printed patterns also plays a critical role in this case. On a low hysteresis island, for example pure paraffin, the droplet can continue to recede past the edge of the pattern and droplet splitting occurs in a small contact area. By increasing the hysteresis of the pattern, droplet pinning is promoted across a larger surface area

Fig. 9 Sampled droplet volume as a function of the grit number of the sandpaper used to impart roughness. *Gray data point* represents measurement made on unmodified carnauba sample. Wax dots of 2 mm diameter were used for these experiments

of the printed dot, which leads to greater adhesion forces, and thus larger droplet volumes after splitting. The images in Fig. 6 show an increase in the droplet contact area as the hysteresis increases due to the pinning action of the increased hysteresis. While the CA hysteresis of the printed dots can theoretically be increased to 180°, its effect on the sampled volume is limited. At a hysteresis of ~60°, the sampled droplet is already pinned at the circumference of the wax pattern, as seen in Fig. 6. Without increasing the area of the printed dot, no additional force can be applied by the island to promote droplet sampling. Figure 9 shows that although the hysteresis is increased from 53.6°±3.9° to

Fig. 8 Advancing and receding CAs, along with CA hysteresis of carnauba wax impregnated substrates that were pressed onto various grades of sandpaper. *Gray data points* represent measurements made on unmodified carnauba samples

Fig. 10 Plot of sampled volume versus hysteresis of chemically and physically modified samples
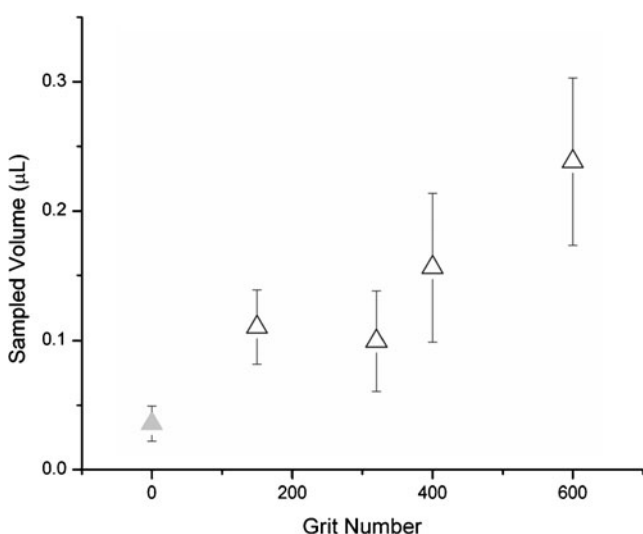
Fig. 11 Images of multiple dot designs fabricated with carnauba wax and **a** unmodified, **b** pressed with 320 grit sandpaper, and **c** pressed with 600 grit sandpaper

$63.9°\pm7.0°$, the sampled volume is not increased between 600 and 1,200 grit pressed samples.

Similarly, it is anticipated that as the dot size is decreased, a limit will be reached where the droplet cannot be split, since the dot does not provide sufficient adhesion force to overcome the surface tension force of the bulk droplet as it deforms. Below this minimum radius, regardless of the hysteresis, the dot is unable to sufficiently deform the droplet to cause sampling. Experimentally, this minimum could not be determined using carnauba wax due to resolution limitations of the printing technique and stamp fabrication. Calculation of the minimum dot size is a nontrivial task due to the complexity of the droplet breakup dynamics, which strongly depends on the shape and curvature of the deformed drop prior to breakup. Nevertheless, the existence of a minimum dot size was proven by using higher resolution printed wax dots created with a Xerox Phaser 8650 printer; in these experiments with a commercial, proprietary wax mixture, it was observed that a dot size of 150 μm was too small to enable fluid sampling.

Multi-dot sampling

The ability to control sampled droplet volume by printing high hysteresis patterns onto low hysteresis SH paper is not limited to the relatively simple single-dot designs presented above. Adjusting the design to include five dots by using the stamp in Fig. 2, bulk droplets can be split into five samples, as shown in Fig. 11. The multiple-dot wax design has a larger 2-mm diameter wax island in the center, and four smaller 1-mm diameter wax islands surrounding it. The size difference between the central and surrounding islands is important for the uniformity and reproducibility of the droplet splitting process. As the patterned substrate is pulled away from the bulk droplet, the liquid recedes along the top surface. Further separation between the sheets causes the droplet to become pinned and split at each printed dot, one at a time, until the droplet is only attached to top substrate in one location. After this point, any further separation between the substrates will cause a final split that fully detaches the bulk droplet from the patterned substrate. The receding liquid will release last from the printed wax feature on the top substrate that provides the strongest adhesion; by purposely placing a larger dot in the center of the multi-dot design, the release process is stabilized and uniform droplet splitting is realized from the outer islands. As expected, adding physical roughness to the wax islands by pressing the multi-dot patterns onto sandpaper again correlates to an increase in sampled volume, as shown in Fig. 12.

The ability to split single bulk droplets into several smaller sample droplets of well-defined volume permits the use of paper substrates in HELP applications. Martinez and coworkers have investigated the use of paper substrates for point-of-care biomedical testing [34, 35] through the fabrication of microfluidic devices. In these studies, lithographic techniques were used to create isolated hydrophilic cellulose channels with hydrophobic barriers between them. Fluids were then wicked into the paper via capillary flow towards reagents at the ends of the channels. Paper is inexpensive, biodegradable and available worldwide, making it an attractive substrate for these one-time-use biomedical applications. Using HELP techniques, colorimetric reagents can be either deposited on the high hysteresis islands or chemically incorporated into the islands themselves. Incorporation of the reagents into the island, for example via grafting or noncovalent specific binding interactions, would enable testing of nontransparent liquids, such as blood, because a post-test washing step can be performed. Figure 13 shows a
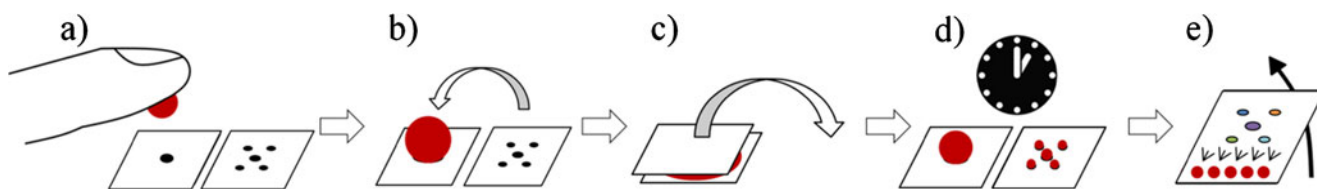

Fig. 12 Plot of volume sampled versus grit for the 4-perimeter island in a multiple dot design. *Gray data point* represents measurement made on unmodified carnauba sample

Fig. 13 Procedure for HELP biomedical testing: **a** patient places droplet of blood on SH sheet, **b** compress blood droplet using another SH sheet with a colorimetric design array, **c** remove colorimetric sheet (difference in CA hysteresis allows sampling), **d** wait for reaction to occur, and **e** remove blood droplets from design array and view diagnosis through colorimetric changes

proposed procedure for the splitting and testing of a blood sample. If the colorimetric reagents are not incorporated into the island, step e) would be impossible and a transparent liquid would be needed to properly gauge a colorimetric change.

To demonstrate the capacity of HELP techniques to enable colorimetric biochemical tests, a glucose immunoassay was conducted. The testing of glucose concentrations in blood and urine is a well-developed technique, extensively studied in the 1940s [36]. The immunoassay uses chemical reagents that result in a change in color intensity, the magnitude of which can be correlated to glucose concentration. By drying glucose colorimetric reagents on each perimeter island and then sampling from bulk droplets of our test liquids (DI water and glucose solutions at 0.0015 and 0.005 M; see Fig. 14), the ability of the HELP technique to perform colorimetric tests can be assessed. This technique can easily be extended to other immunoassays with the advantage that each island of the multi-dot pattern can be treated with a different reagent, thus enabling different tests to be simultaneously performed on a single substrate. Additionally, with the ability to control the volume of the sampled droplets through hysteresis, it is possible to tune the volumes of the droplets sampled by each island separately, depending upon the requirements of the biological test.

Conclusion

The ability to control the volume of water droplets split from a bulk drop using high hysteresis wax islands printed on low hysteresis SH paper has been demonstrated. The volume sampled is dependent on the magnitude of the wax island hysteresis. Chemically, hysteresis was adjusted through control of the active chemical groups present on the surface of the printed island. Physical hysteresis was controlled through the addition of surface roughness by pressing various grades of sandpaper into the wax surface without affecting the surface chemistry. A good correlation was observed between the sampled volume and the hysteresis, independent of the method of hysteresis modification. The increase in sampled volume with increasing hysteresis is due to the force balance that evolves during the droplet splitting process. By increasing the hysteresis the droplet is pinned to a higher surface area of the wax island, resulting in stronger adhesion and a higher sampled volume.

Control of the volume of sample droplets through physical hysteresis modification was extended to the simultaneous extraction of multiple sample droplets from a single bulk droplet by using a more complicated multi-dot array on the top substrate. The reproducibility of this technique for splitting off droplets with a well-defined volume from a bulk droplet of test liquid enables quantitative colorimetric biomedical tests, as we demonstrated by performing a colorimetric glucose immunoassay. These studies indicate that by applying different colorimetric reagents to each island, it will be possible to perform multiple biomedical tests simultaneously on a single lab-on-paper device. The ability to control volume also enables the integration of immunoassays with varying volume requirements, thereby allowing multiple quantitative analyses to be performed on the same substrate..
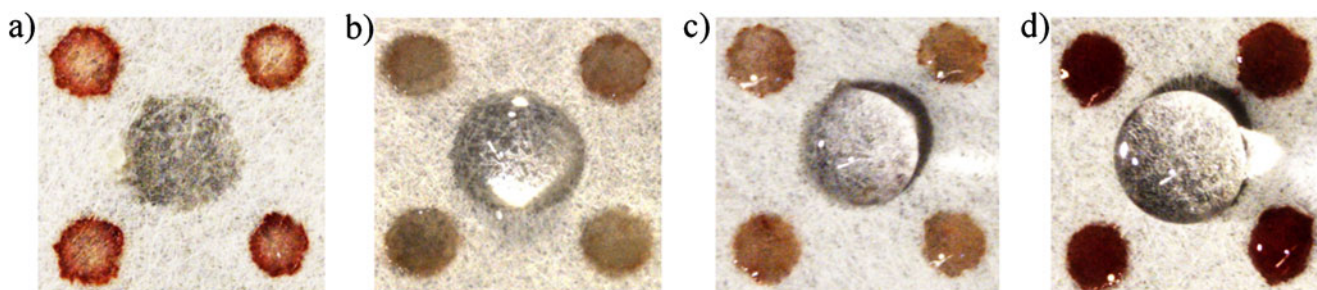
Fig. 14 Colorimetric glucose test performed with high hysteresis islands on SH paper substrates; **a** dried reagents before exposure to test liquid; after sampling from bulk drops of **b** DI water, **c** 0.0015 M glucose solution, and **d** 0.005 M glucose solution

References

1. Callies M, Quere D (2005) On water repellency. Soft Matter 1 (1):55–61. doi:10.1039/b501657f
2. Mertaniemi H, Jokinen V, Sainiemi L, Franssila S, Marmur A, Ikkala O, Ras RHA (2011) Superhydrophobic tracks for low-friction, guided transport of water droplets. Adv Mater 23:2911–2914
3. Li XM, Reinhoudt D, Crego-Calama M (2007) What do we need for a superhydrophobic surface? A review on the recent progress in the preparation of superhydrophobic surfaces. Chem Soc Rev 36 (8):1350–1368. doi:10.1039/b602486f
4. Quere D (2008) Wetting and roughness. Ann Rev Mater Res 38:71–99. doi:10.1146/annurev.matsci.38.060407.132434
5. Xia F, Jiang L (2008) Bio-inspired, smart, multiscale interfacial materials. Adv Mater 20(15):2842–2858. doi:10.1002/adma.200800836
6. Roach P, Shirtcliffe NJ, Newton MI (2008) Progess in superhydrophobic surface development. Soft Matter 4(2):224–240. doi:10.1039/b712575p
7. Carré A, Mittal KLE (2009) Superhydrophobic surfaces. VSP/Brill, Leiden
8. Barthlott W, Neinhuis C (1997) Purity of the sacred lotus, or escape from contamination in biological surfaces. Planta 202 (1):1–8
9. Cheng YT, Rodak DE (2005) Is the lotus leaf superhydrophobic? Appl Phys Letters 86(14):144101. doi:10.1063/1.1895487
10. Jiang L, Zhao Y, Zhai J (2004) A lotus-leaf-like superhydrophobic surface: a porous microsphere/nanofiber composite film prepared by electrohydrodynamics. Angew Chem Int Edit 43(33):4338–4341. doi:10.1002/anie.200460333
11. Sun TL, Feng L, Gao XF, Jiang L (2005) Bioinspired surfaces with special wettability. Acc Chem Res 38(8):644–652. doi:10.1021/ar040224c
12. Feng L, Zhang Y, Xi J, Zhu Y, Wang N, Xia F, Jiang L (2008) Petal effect: a superhydrophobic state with high adhesive force. Langmuir 24(8):4114–4119. doi:10.1021/la703821h
13. Furstner R, Barthlott W, Neinhuis C, Walzel P (2005) Wetting and self-cleaning properties of artificial superhydrophobic surfaces. Langmuir 21(3):956–961. doi:10.1021/la0401011
14. McHale G, Shirtcliffe NJ, Newton MI (2004) Contact-angle hysteresis on super-hydrophobic surfaces. Langmuir 20(23):10146–10149. doi:10.1021/la0486584
15. Xiu Y, Zhu L, Hess DW, Wong CP (2007) Hierarchical silicon etched structures for controlled hydrophobicity/superhydrophobicity. Nano Lett 7(11):3388–3393. doi:10.1021/nl0717457
16. Safaee A, Sarkar DK, Farzaneh M (2008) Superhydrophobic properties of silver-coated films on copper surface by galvanic exchange reaction. Appl Surface Sci 254(8):2493–2498. doi:10.1016/j.apsusc.2007.09.073
17. Qian BT, Shen ZQ (2005) Fabrication of superhydrophobic surfaces by dislocation-selective chemical etching on aluminum, copper, and zinc substrates. Langmuir 21(20):9007–9009. doi:10.1021/la051308c
18. Shiu JY, Kuo CW, Chen PL, Mou CY (2004) Fabrication of tunable superhydrophobic surfaces by nanosphere lithography. Chem Mater 16(4):561–564. doi:10.1021/cm034696h
19. Morra M, Occhiello E, Garbassi F (1989) Contact-angle hysteresis in oxygen plasma treated poly(tetrafluoroethylene). Langmuir 5 (3):872–876. doi:10.1021/la00087a050
20. Balu B, Breedveld V, Hess DW (2008) Fabrication of "roll-off" and "sticky" superhydrophobic cellulose surfaces via plasma processing. Langmuir 24(9):4785–4790. doi:10.1021/la703766c
21. Balu B, Kim JS, Breedveld V, Hess DW (2009) Tunability of the adhesion of water drops on a superhydrophobic paper surface via selective plasma etching. J Adhesion Sci Technol 23(2):361–380. doi:10.1163/156856108x383547
22. Israelachvili JN (2010) Intermolecular and surface forces, 3rd edn. Elsevier, Amsterdam
23. Chen YL, Helm CA, Israelachvili JN (1991) Molecular mechanisms associated with adhesion and contact-angle hysteresis of monolayer surface. J Phys Chem 95(26):10736–10747. doi:10.1021/j100179a041
24. Barona D, Amirfazli A (2011) Producing a superhydrophobic paper and altering its repellency through ink-jet printing. Lab on a Chip 11(5):936–940. doi:10.1039/c0lc00335b
25. Wang CF, Wang TF, Liao CS, Kuo SW, Lin HC (2011) Using pencil drawing to pattern robust superhydrophobic surfaces to control the mobility of water droplets. J Phys Chem 115 (33):16495–16500. doi:10.1021/jp204169p
26. Leopoldes J, Dupuis A, Bucknall DG, Yeomans JM (2003) Jetting micron-scale droplets onto chemically heterogeneous surfaces. Langmuir 19(23):9818–9822. doi:10.1021/la0353069
27. Balu B, Berry AD, Hess DW, Breedveld V (2009) Patterning of superhydrophobic paper to control the mobility of micro-liter drops for two-dimensional lab-on-paper applications. Lab on a Chip 9(21):3066–3075. doi:10.1039/b909868b
28. Balu B, Berry AD, Patel KT, Breedveld V, Hess DW (2011) Directional mobility and adhesion of water drops on patterned superhydrophobic surfaces. J Adhesion Sci Technol 25(6–7):627–642. doi:10.1163/016942410x525849
29. Sokoll LJ, Chan DW (1999) Clinical analyzers. Immunoassays. Anal Chem 71(12):356R–362R
30. Ferris SW, Cowles JHC, Henderson LM (1929) Composition of paraffin wax. Ind Eng Chem 21(11):3
31. Vandenburg LE, Wilder EA (1970) The structural constituents of carnauba wax. J Amer Oil Chemists' Soc 47(12):514
32. Dettre RH, Johnson RE Jr (1964) Contact angle hysteresis. Am Chem Soc 43(43):136–144. doi:10.1021/ba-1964-0043.ch008
33. Bhushan B, Nosonovsky M, Jung YC (2007) Towards optimization of patterned superhydrophobic surfaces. J Royal Soc Interface 4(15):643–648. doi:10.1098/rsif.2006.0211
34. Martinez AW, Phillips ST, Butte MJ, Whitesides GM (2007) Patterned paper as a platform for inexpensive, low-volume, portable bioassays. Angew Chem Int Edit 46(8):1318–1320. doi:10.1002/anie.200603817
35. Martinez AW, Phillips ST, Whitesides GM (2008) Three-dimensional microfluidic devices fabricated in layered paper and tape. Proc Natl Acad Sci USA 105(50):19606–19611. doi:10.1073/pnas.0810903105
36. King EJ, Garner RJ (1947) The colorimetric determination of glucose. J Clin Pathol 1(1):30–33. doi:10.1136/jcp.1.1.30